Effect of pH on the Electrochemical Properties of Oxides formed over β – Ti-15Mo and Mixed Ti-6Al-4V Alloys

Shaily M. Bhola and *Brajendra Mishra*

Department of Metallurgical and Materials Engineering;
Colorado School of Mines, Golden, CO, USA-80401
*E-mail: malhotra.shaily@gmail.com

In the present study, the role of pH on the corrosion behavior of two titanium alloys, beta Ti-15Mo and mixed Ti-6Al-4V has been examined in phosphate buffer saline solution at the open circuit potential (OCP) and at 1 V vs. SCE anodic potential. The techniques involved were Open Circuit Potential (OCP), Electrochemical Impedance Spectroscopy (EIS) and Potentiodynamic Polarization. The electrochemical parameters evaluated from these techniques such as polarization resistance (R_p), inhomogeneity parameter (n), thickness of oxide (d) and corrosion current density (I_{corr}) have been used to interpret results.

1. INTRODUCTION

Titanium and its alloys are the most promising metallic materials for use as implants due to their remarkable mechanical properties, excellent corrosion resistance and biocompatibility. Ti-6Al-4V is a traditional titanium alloy and the most preferred choice for a biomaterial because of its good corrosion resistance and mechanical properties closer to that of bone [1-2]. However, aluminium and vanadium ions have been associated with various adverse reactions and disorders as per the findings from recent studies [3-6]. In the last few years, titanium alloys without Al and V have been developed and the focus has been on the low modulus alloys containing beta phase stabilizing elements such as Nb, Ta, Zr and Mo [7-8].

In spite of the favorable properties of titanium alloys for biomaterial applications, they can still release metal ions into the tissue surrounding the implant, which react with the human fluid, especially with chloride ions forming complexes and precipitates. They also can form hydroxides or oxides with

water and produce the local change of the pH [9-11]. These pH changes can cause the local acceleration of corrosion reaction on some areas of the implant. Moreover, during an inflammatory reaction, the pH can vary from 5.4 until 7.8 [12].

The intraoral environment is hostile due to corrosive and mechanical actions. It is continuously full of saliva, an aerated aqueous solution of chloride with varying amounts of Na^+, K^+, Ca^{2+}, PO_4^{3-}, CO_3^{2-}, sulfur compounds and mucin. The pH value is normally in the range 6.5-7.5 but under plaque deposits it may be as low as 2.0. A variety of food and drink concentrations with pH ranging from 2.0 to 14.0, stay inside the mouth for short periods of time [13]. According to Black [14], the potential of a metallic biomaterial can range from -1 to 1.2 V versus SCE in the human body.

The aim of this study is to investigate and compare the influence of pH on the corrosion behavior of two titanium alloys, beta Ti-15Mo and mixed Ti-6Al-4V, in a phosphate buffer saline solution using electrochemical techniques.

2. MATERIALS AND METHODS

2.1. Materials preparation

Titanium alloys, Ti-15Mo (0.05%C, 0.1%Fe, 0.015%H, 0.01%N, 0.15%O, 15%Mo & 84.67%Ti) and Ti-6Al-4V (0.1%C, 0.2%Fe, 0.015%H, 0.03%N, 0.2%O, 6%Al, 4%V & 89.45%Ti) were used for the present investigation. The specimens were finished with different grades of SiC grit papers (2400 grit max), polished over the diamond abrasive wheel (0.25 μm diamond paste) and washed with acetone.

The simulated body fluid used was 1X phosphate buffer saline (PBS) solution (composition of 10x PBS: 0.137 M sodium chloride, 0.0027 M potassium chloride and 0.01 M phosphate buffer) of pH 6.5. pH values of the 1X PBS solution were adjusted to 2.5, 3.1, 4, 5.36, 8, 9.1, 10.62 and 11.63 using 1N HCl and 1N NaOH.

2.2. Measurements

A three-electrode cell assembly consisting of titanium alloy as the working electrode, platinum wire as the counter electrode and a saturated calomel electrode (SCE) as the reference electrode was used for the corrosion measurements. Electrochemical testing was performed at 298 K under naturally aerated conditions in a closed system in the following sequence:

Open circuit potential (OCP): OCP of the working electrode was allowed to stabilize for 1 hour.

Electrochemical impedance spectroscopy (EIS): Impedance measurements were performed at the open circuit potential using a PAR 1255 FRA. The frequency sweep was applied from 10^5 to 10^{-2} Hz with the AC amplitude of 10 mV.

Potentiodynamic polarization: Potentiodynamic polarization measurements were performed using a PAR Potentiostat 273A, by polarizing the working electrode from an initial potential of -500

mV vs. OCP, upto a final potential of 1 V vs. SCE. A scan rate of 0.1667 mV/s was used for the polarization sweep.

Potentiostatic polarization: The working electrode was potentiostatically polarized at 1 V for 1 hour.

EIS: Impedance measurements were again performed at 1 V. The frequency sweep was applied from 10^5 to 10^{-2} Hz with AC amplitude of 10 mV.

OCP: The circuit was open and OCP was allowed to stabilize for 1 hour.

3. RESULTS AND DISCUSSION

Fig. 1 shows the OCP-pH curves for Ti-15Mo and Ti-6Al-4V alloys. The stabilized OCPs of the electrodes at one hour of immersion have been plotted together with the stabilized OCP values obtained when the sequence of experiments, as described above, was complete and the circuit was open. The former OCP values have been denoted as pre-polarization OCPs (pre-pol) and later ones as post-polarization OCPs (post-pol). The pre-polarization OCPs are the potentials the Ti alloy attains after remaining immersed in the PBS solution for an hour. The post-polarization OCPs are the potentials the Ti alloy attains after it gets polarized at a potential of 1V and the oxide film is allowed to potentiostatically grow for an hour at 1V. It is well known that under open circuit conditions and at potentials in the passivation range, the primary oxide formed over titanium alloys is TiO_2, as also shown in the Pourbaix diagrams in Figs. 2 a & b.
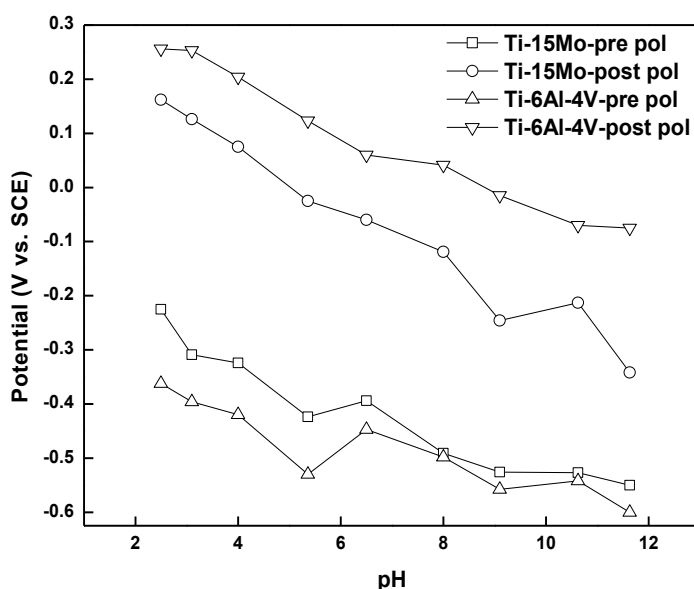
Figure 1. Pre- and post-polarized OCP values for Ti-15Mo and Ti-6Al-4V as a function of pH

In case of Ti-15Mo alloy in Fig. 1, the post-pol OCPs are more positive than the pre-pol OCPs. This implies that the oxide film grown over Ti-15Mo alloy at 1V potential has better barrier properties and is thermodynamically more stable compared to the oxide film formed under unpolarized

conditions. At pH values below 6.5, which is the pH of 1X PBS solution, the OCP values become more positive as pH decreases and at pH values above 6.5, the OCP values become less positive as pH increases. The reason for this behavior will be explored in the potentiodynamic results section. The OCP-pH trend for Ti-6Al-4V alloy follows a similar behavior.
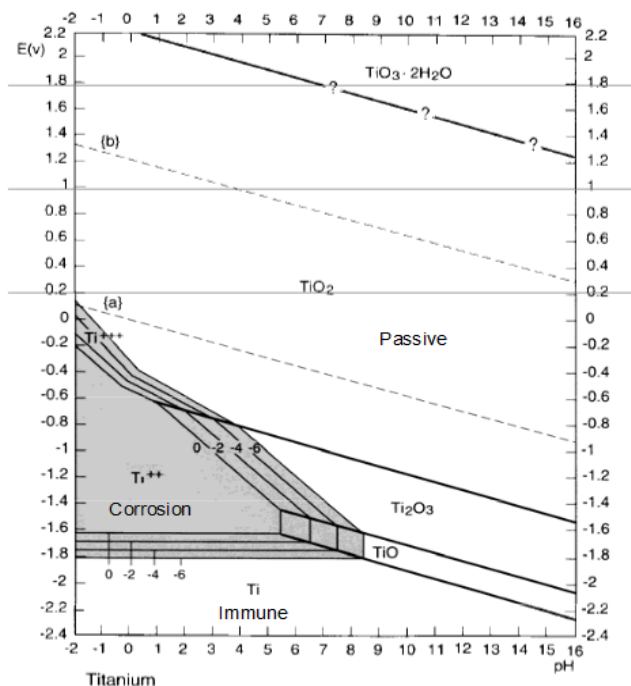
Figure 2a. Pourbaix diagram for the Ti-H_2O system at 25 °C [15]
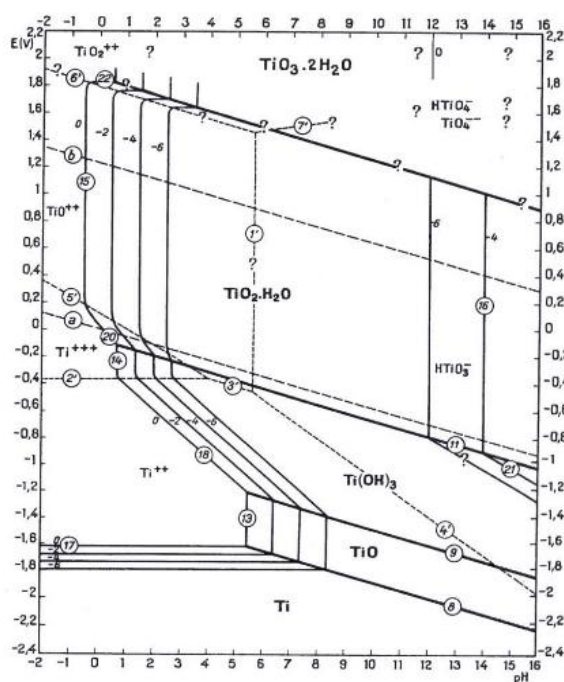
Figure 2b. Potential-pH (Pourbaix) Diagram for the Titanium-Water System at 25 °C(Assuming TiO_2 .H_2O to be the Stable Solid Phase) [16]

Another point to note in Fig. 1 is the gap between the pre-pol OCPs and post-pol OCPs which is greater for Ti-6Al-4V than for Ti-15Mo alloy. This means that the film formed over Ti-6Al-4V alloy has better passivation characteristics than the film formed over Ti-15Mo alloy.

EIS response of Ti-15Mo and Ti-6Al-4V alloys showed one time constant behavior and the data followed the circuit model shown in Fig. 3, where R_s is the solution resistance, R_p is the polarization resistance and CPE is the constant phase element for the capacitance of the passive oxide film. The impedance of the CPE is given by,

$$Z\ (CPE) = [Q\ (j\omega)^n]^{-1} \tag{1}$$

where, Q is the constant of CPE, ω is the angular frequency in rad s^{-1} and n is the exponential term which can vary between 1 for pure capacitance and 0 for a pure resistor [17]. n is a measure of surface inhomogeneity; the lower is its value, the higher is the surface roughening of the metal/alloy [18].
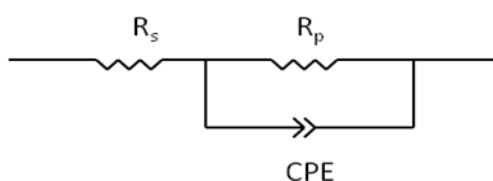
Figure 3. Circuit model used to fit EIS data for Ti-15Mo and Ti-6Al-4V alloys

Figs. 4 a & b show the EIS plots for Ti-15Mo alloy at pH values 2.5, 6.5 and 11.63 obtained at the pre-pol OCP and at 1 V respectively. To avoid redundant use of terms, the term 'pre-pol OCP' has been retained as OCP in the rest of the paper. To make the curves appear clearer and less-overlapping, these have been shown at selected pH values. On comparing the plots in Figs. 4a and 4b, it can be noted that at OCP, there is not much change in the appearance of the Bode curves, whereas, at 1 V potential, the shape of the Bode curve at pH 11.63 is quite different from the Bode curves at other two pH values. The diameter of the semicircle and the impedance modulus at the low frequency end give the information about the interfacial properties of the alloy in terms of its polarization resistance. At pH 2.5 and 6.5 in Fig. 4b, the phase angle curves show a near-capacitive behavior in the intermediate frequency range (phase angles being less than -90°), with phase angles dropping to -25° at the low frequency end. At pH 11.63, the phase angle curve shows a decrease to 0° value at the low frequency end and correspondingly the impedance modulus curve shows a horizontal region at low frequencies, which is indicative of the response of a resistor. In this case, the Nyquist curve shows a small diameter, compared to the curves at other two pH values. The slopes of Z_{mod}-frequency curves and the values of phase angles in the intermediate frequency range for Ti-15Mo alloy at OCP are between -0.86 to -0.89 and -78° to -81° respectively. At 1 V, these values are between -0.88 to -0.94 and around -84°. The deviation of the slope values from -1 and phase angles from -90° explains the deviation from an ideal capacitive behavior of the oxide film. The inhomogeneity parameter values were less than 1 (Fig. 8), which also reveals the porous character of the passive oxide film.

(a) at OCP

(b) at 1 V
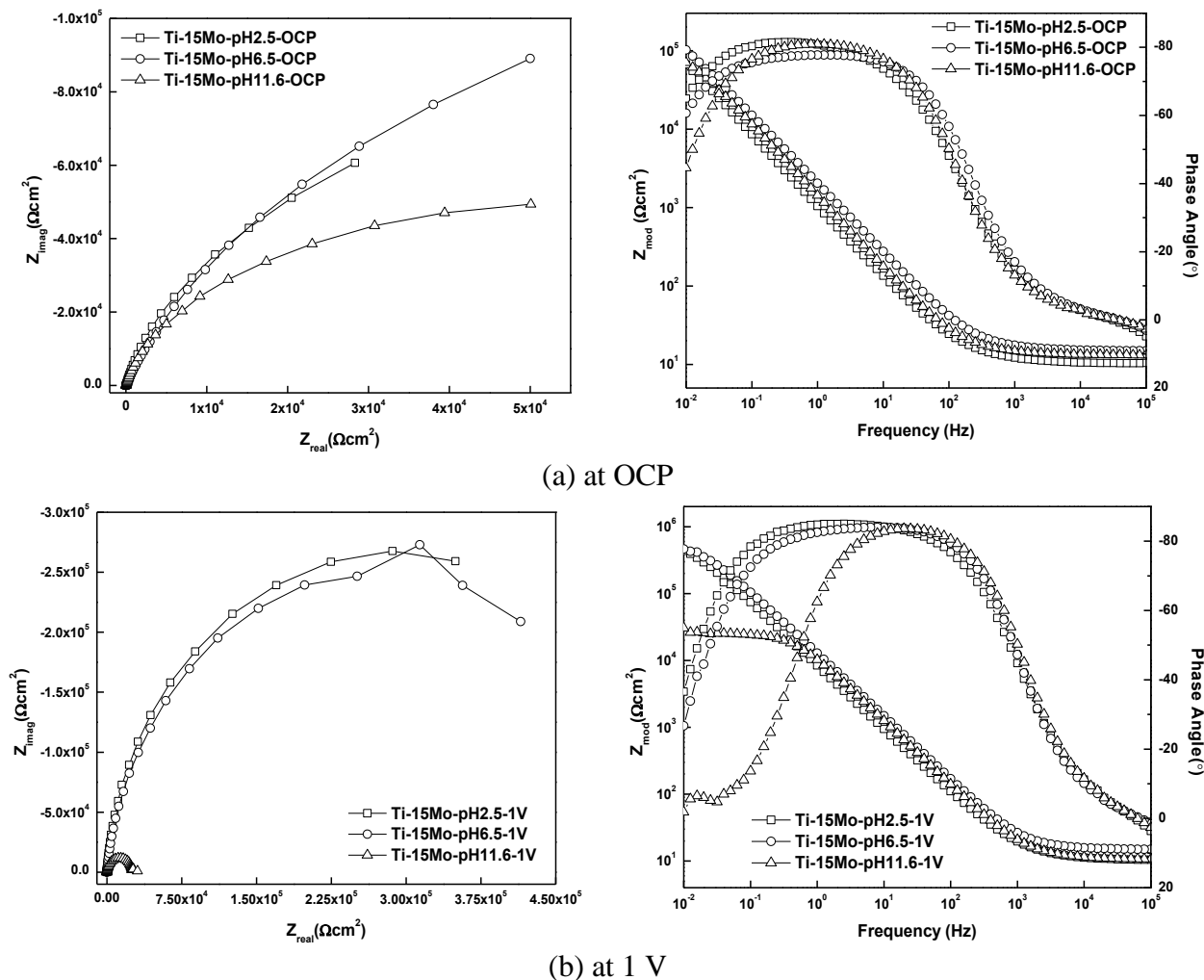
Figure 4. Nyquist and Bode plots for Ti-15Mo alloy in PBS solution

Figs. 5 a & b show the EIS plots for Ti-6Al-4V alloy at pH values 2.5, 6.5 and 11.63 obtained at OCP and at 1 V respectively. A similar behavior to Ti-15Mo alloy was observed in this case at both OCP and 1 V potential. The slopes of Z_{mod}-frequency curves and the values of phase angles in the intermediate frequency range for Ti-6Al-4V alloy at OCP are between -0.87 to -0.91 and around -82° respectively. At 1 V, these values are between -0.93 to -0.95 and around -84°.

(a) at OCP

(b) at 1V
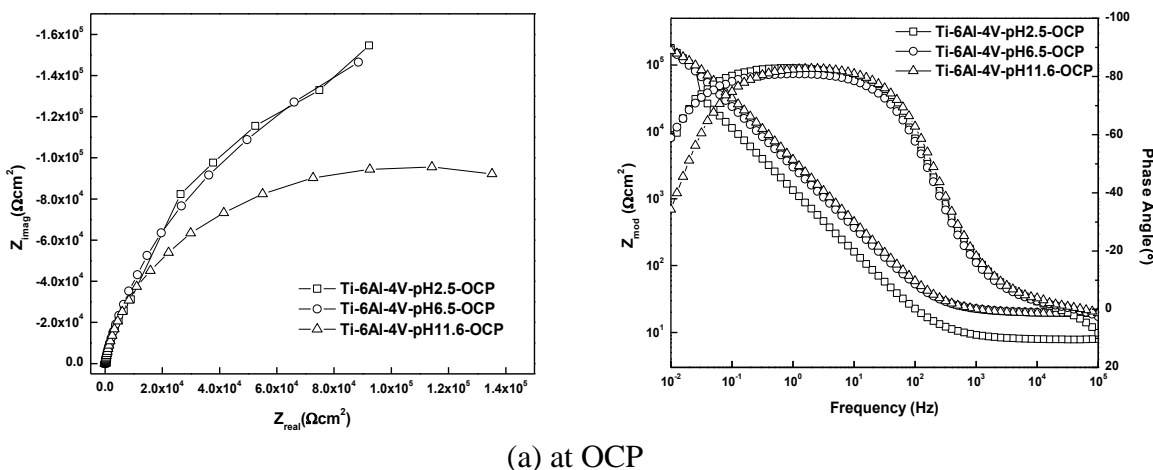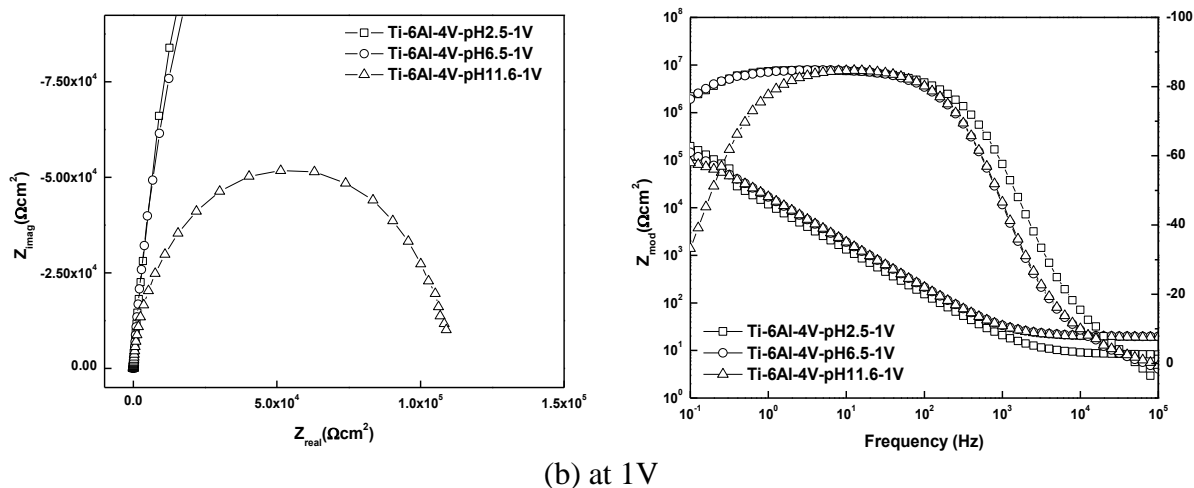
Figure 5. Nyquist and Bode plots for Ti-6Al-4V alloy in PBS solution

Fig. 6 shows the polarization resistance (R_p) values as a function of pH for Ti-15Mo and Ti-6Al-4V alloys at OCP and at 1 V potential. At OCP, the R_p-pH curves are bell shaped and almost symmetrical about pH 6.5. At 1 V potential, the curves are still bell-shaped but give an unsymmetrical appearance, with the apex shifted to pH 4. At pH values below the apex pH at both potentials, the polarization resistance decreases as the acidity of the solution increases and at pH values above the apex pH, the R_p values also decrease with increase in basicity of the solution. At low pH values, the reduced R_p values can be attributed to the aggressive Cl⁻ ions in the PBS solution that can attack the TiO_2 oxide passive layer [19]. However, in case of the R_p curves at 1 V, the R_p value drops considerably as the pH is increased, matching with the R_p curves at OCP. This means at high pH values, the oxide film formed at 1 V potential loses its protective capacity. This result was also observed in Figs. 4 b and 5 b in the EIS curves. Ti-6Al-4V alloy shows higher R_p values than Ti-15Mo alloy at both OCP and 1 V potential.
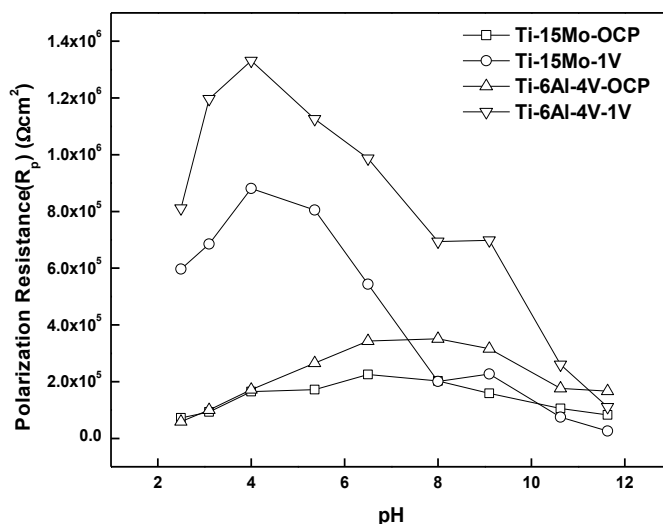
Figure 6. Polarization resistance-pH curves for Ti-15Mo and Ti-6Al-4V alloys
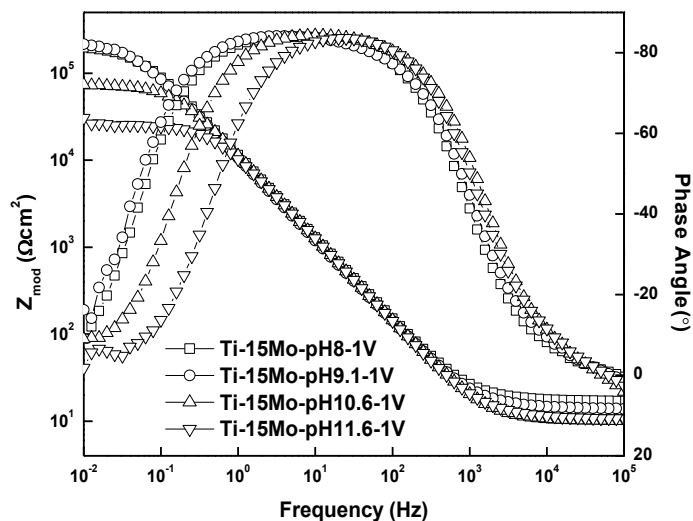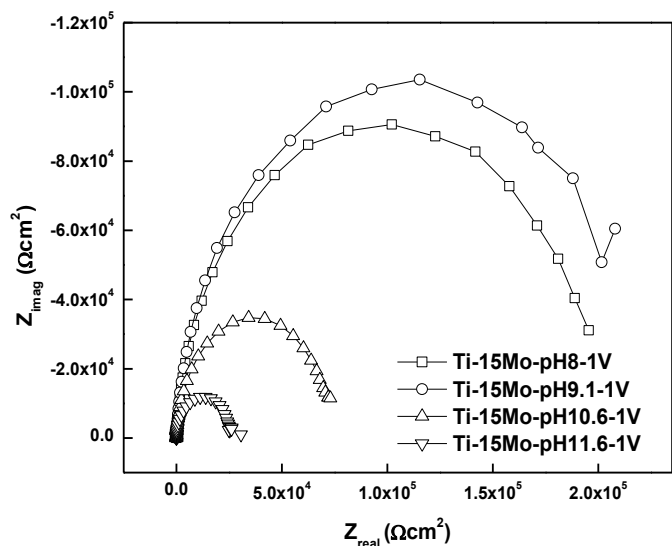
(a) Ti15Mo
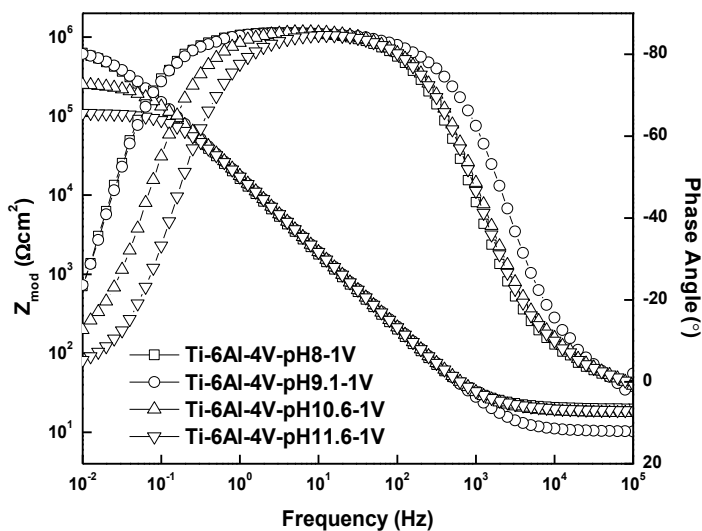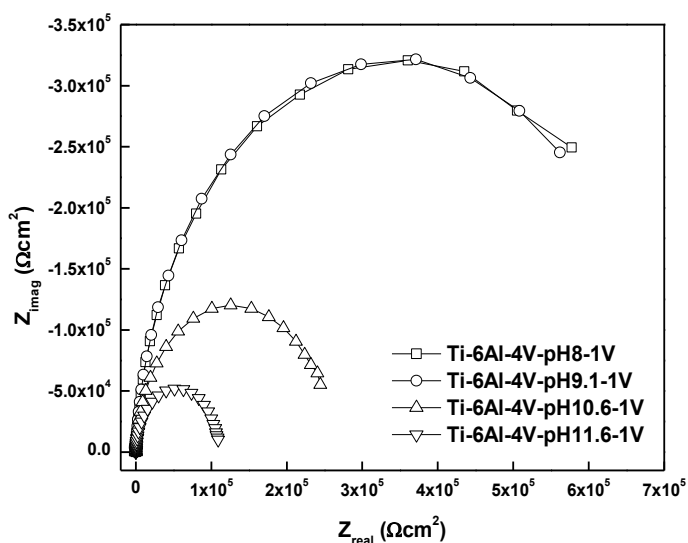
(b) Ti64

Figure 7. Nyquist and Bode plots for Ti-15Mo and Ti-6Al-4V alloys in PBS solution at high pH values

It can also be noted from Fig. 6 that R_p values for Ti-15Mo alloy at 1 V potential and at pH 10.62 and 11.63 are lower than the corresponding R_p values at OCP. For Ti-6Al-4V alloy, R_p at 1 V and pH 11.63 is lower than the R_p at OCP. The observed lower value of R_p at an anodic potential compared to that at OCP is only possible if there is breakdown of the passive film. The reason will be explored in the potentiodynamic results section. Since the R_p-pH curves at 1 V potential for the two alloys show a significant decrease in R_p with increase in pH starting at pH 8, the Figs. 7 a-b show the EIS curves for alloys Ti-15Mo and Ti-6Al-4V respectively at pH values 8, 9.1, 10.62 and 11.63. As the pH is increased, the semicircle diameter of the Nyquist curve decreases, the low frequency horizontal region (resistive behavior) increases in the Z_{mod} curve with decreasing Z_{mod} values at the low frequency end, the intermediate frequency region in the Z_{mod} curve (capacitive behavior) decreases and the

intermediate frequency horizontal region in the phase angle curve (capacitive behavior) decreases. The phase angles reach a 0° value at the low frequency end at 10^{-2} Hz frequency.The values of the inhomogeneity parameter, n, for both the alloys have been plotted at OCP and 1 V potential in Fig. 8. The higher n values at 1 V show that the oxide film formed at the higher potential in the passivation region is more compact and less defective. The n values at OCP are higher for Ti-6Al-4V than Ti-15Mo alloy and at 1 V, the values are similar.
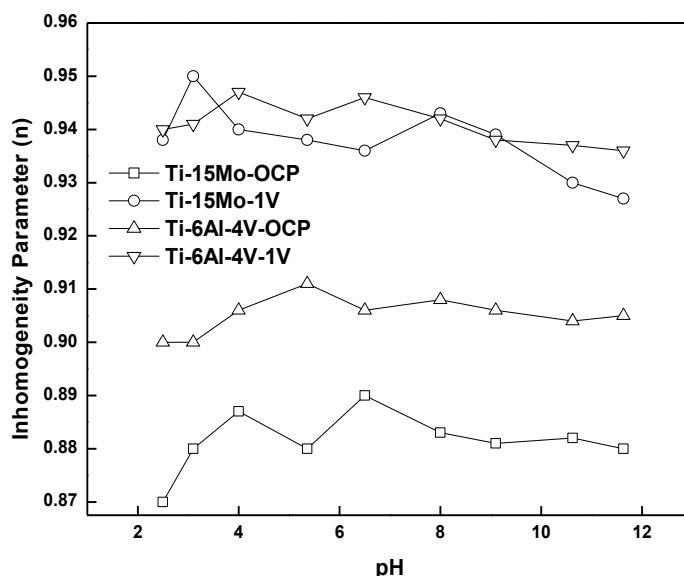
Figure 8. Inhomogeneity parameter as a function of pH for Ti-15Mo and Ti-6Al-4V alloys in PBS solution

From the capacities obtained at different pH values, the thickness of the oxide layer was calculated using the expression [20]:

$$d = \varepsilon\varepsilon_0 A/C \qquad \qquad \text{-(2)}$$

where, d is the oxide layer thickness, A is the surface area, C is the oxide layer capacitance, ε is the dielectric constant of the oxide and ε_0 is the permittivity of free space (= 8.85 x 10^{-12} F m^{-1}). The thickness values for both alloys have been plotted as a function of pH in Fig. 9. The thickness of the oxide film formed over Ti-15Mo alloy at 1 V potential has increased to a value between 2 and 3 nm from a value between 0.25 to 0.45 nm at OCP. For Ti-6Al-4V alloy, the oxide thickness has increased to a value between 3 and 4.5 nm at 1 V from a value between 0.3 and 0.9 nm at OCP. The oxide thickness values are higher for Ti-6Al-4V at both OCP and 1 V than for Ti-15Mo alloy.

Figs. 10 a-b show the potentiodynamic polarization curves for Ti-15Mo and Ti-6Al-4V alloys at various selected pH values. At all pH values except 10.62 and 11.63, Ti-15Mo alloy was passivated at the chosen anodic potential of 1 V for evaluating oxide film characteristics. This can be observed in the potentiodynamic curves of Ti-15Mo alloy at pH 2.5 and 6.5. However, at pH 10.62 and 11.63, it can be noticed in Fig. 10a that the polarization curve is no more independent of current density (as in the passivation range) but shows an increase in current density above somewhere around 0.75-0.8 V. This is suggestive of the breakdown of the passive oxide film and initiation of pitting. This result is in

correlation with the observed lower R_p values at 1 V (Fig. 6) at the two pH values mentioned above. In case of Ti-6Al-4V alloy, the breakdown of oxide occurs at pH 11.63 at 0.8 V. This explains the lower Rp value at 1 V potential and pH 11.63 in Fig. 6. At all other pH values, the polarization curves showed passivation behavior even up to a potential of 1 V.
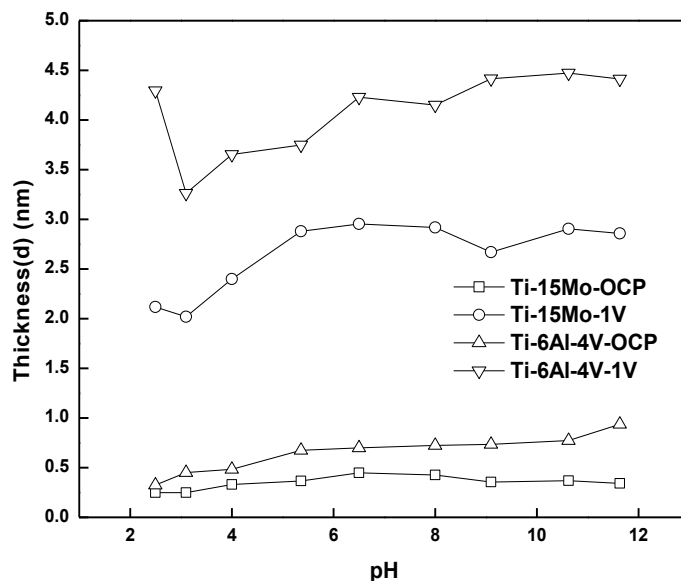
Figure 9. Thickness values for Ti-15Mo and Ti-6Al-4V alloys in PBS solution as a function of pH

The observed breakdown of passivity for the two alloys indicates that at these high pH values and at an anodic potential of around 0.8 V, TiO_2 passive film breaks to produce $HTiO_3^-$ ions in solution (Fig. 2b).

The polarization curves at other pH values that have not been shown in Figs. 10 a-b did not show any different information and they have been excluded in order to make the other curves appear comprehensible.

It is well known that in case of titanium, the growth of the oxide film begins mainly as TiO_2 in the active anodic region [20-24]:

$$Ti + 2H_2O \rightarrow TiO_2 + 4H^+ + 4e^- \qquad \text{-(3)}$$

In the cathodic region, the following reactions are possible in aqueous solution:

$$2H^+ + 2e^- \rightarrow H_2 \text{ (acidic, deaerated solution)} \qquad \text{-(4)}$$

$$2H_2O + 2e^- \rightarrow H_2 + 2OH^- \text{ (basic/neutral deaerated solution)} \qquad \text{-(5)}$$

$$4H^+ + 4e^- + O_2 \rightarrow 2H_2O \text{ (acidic, aerated solution)} \qquad \text{-(6)}$$

$$2H_2O + 4e^- + O_2 \rightarrow 4OH^- \text{ (basic/neutral aerated solution)} \qquad \text{-(7)}$$
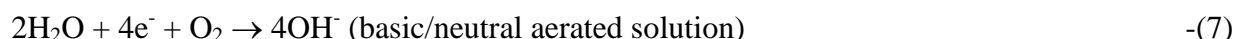
At the open circuit potential, the rates of the cathodic and anodic reactions are equal.

From the above electrochemical reactions, it is clear that as pH is lowered, the rate of cathodic reaction increases and the rate of anodic reaction decreases. This behavior can also be seen in the cathodic and anodic branches at different pH values in the potentiodynamic curves in Figs. 10 (a-b). Moreover, at very low pH, the rate of the cathodic reaction in equation 4 is very spontaneous even

under naturally aerated conditions as in the present study since involvement of O_2 in the reaction is diffusion-limited. This explains the very high cathodic reaction rate at pH 2.5 as seen in Figs. 10 a-b. The changes in the rates of the cathodic and anodic reactions govern the corrosion current density and corrosion potential values [21-23]. The cathodic and anodic rate changes with pH explain the shift of the OCP/E_{corr} values in the noble direction as the pH is decreased. This shift in E_{corr} in the noble direction can also be noticed in the potentiodynamic curves. This shift was also observed in the OCP-pH curves in Fig. 1.

(a)   (b)
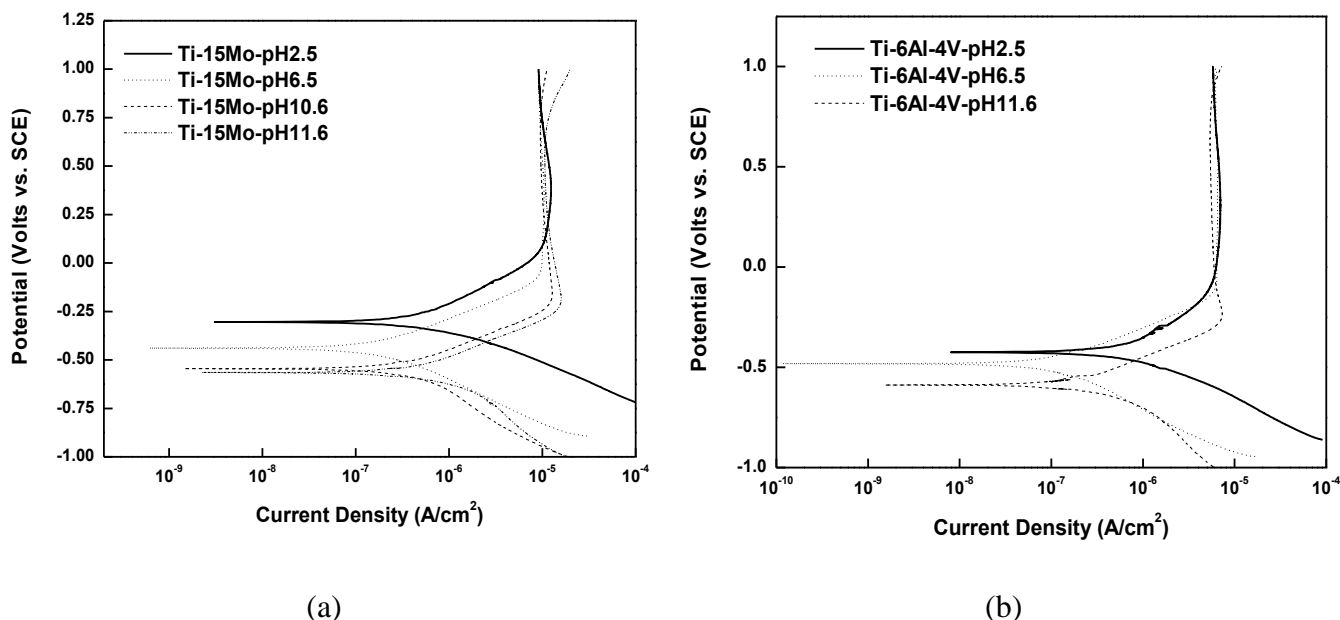
Figure 10. Potentiodynamic polarization curves for (a) Ti-15Mo and (b) Ti-6Al-4V in PBS solution

Table 1. (a) Polarization Parameters For Ti-15Mo Alloy

pH	E_{corr} (V)	I_{corr} (μAcm^{-2})	$-b_c$ (mV per decade)	b_a (mV per decade)	E_{pass} (V)	I_{pass} (μAcm^{-2})
2.5	-0.305	0.361	199	243	0.072	9.591
3.1	-0.400	0.279	201	228	0.018	10.413
4.0	-0.397	0.158	208	221	0.011	8.749
5.36	-0.504	0.151	193	230	-0.094	8.215
6.5	-0.440	0.115	233	191	-0.058	9.283
8.0	-0.527	0.128	250	197	-0.132	9.673
9.1	-0.548	0.164	253	212	-0.137	10.680
10.62	-0.546	0.246	251	189	-0.165	12.730
11.63	-0.566	0.314	324	183	-0.207	15.710

The polarization parameters for the two alloys have been listed in Table 1 (a-b). The I_{corr} values for both the alloys decrease as pH is increased to somewhere between 6.5 and 8 and increase as the pH

values are increased further in the basic pH range. The I_{corr}-pH trend correlates very well with the R_p-pH trend, which followed an exactly reverse behavior. The corrosion current densities for Ti-15Mo alloy are mostly on the higher side as compared to Ti-6Al-4V alloy over the entire pH range studied. The I_{corr} values are in the range 0.11-0.36 μAcm^{-2} for Ti-15Mo and 0.07-0.44 μAcm^{-2} for Ti-6Al-4V alloy. Hsu et al. have reported I_{corr} values in the range 1.25-3.42 μAcm^{-2} for Ti-6Al-4V alloy in PBS solution in the pH range 4-9 at 37 °C [25].The passivation current densities, I_{pass}, are also higher for Ti-15Mo over Ti-6Al-4V alloy, which means that the oxide film formed over Ti-15Mo alloy is defective and porous and the film over Ti-6Al-4V alloy has better passivating characteristics.

Table 1. (b) Polarizaton Parameters For Ti-6Al-4V Alloy

pH	E_{corr} (V)	I_{corr} (μAcm^{-2})	$-b_c$ (mV per decade)	b_a (mV per decade)	E_{pass} (V)	I_{pass} (μAcm^{-2})
2.5	-0.425	0.440	232	244	-0.109	5.270
3.1	-0.470	0.260	224	228	-0.056	5.242
4.0	-0.484	0.151	182	235	-0.062	5.371
5.36	-0.612	0.0982	173	230	-0.170	5.289
6.5	-0.482	0.0761	246	184	-0.108	6.100
8.0	-0.516	0.0743	299	180	-0.145	6.170
9.1	-0.566	0.0825	280	195	-0.179	5.738
10.62	-0.535	0.147	412	175	-0.185	7.480
11.63	-0.588	0.156	435	176	-0.235	7.330

4. CONCLUSIONS

The R_p-pH curve for Ti-15Mo and Ti-6Al-4V alloys in PBS solution was found to follow a bell-shaped behavior at both OCP and 1 V potential, with decreasing R_p values as the pH was moved from the apex to the higher acidity/basicity side. The R_p values were much greater at 1 V than at OCP for the two alloys at low and neutral pH. However, for Ti-15Mo alloy at pH $\geq$ 10.62 and for Ti-6Al-4V alloy at pH 11.63, the R_p values at 1 V were lower than the R_p values at OCP were not much different from each other. This was due to the breakdown of passive oxide film, which was revealed from potentiodynamic measurements. The inhomogeneity parameter and thickness values were also greater at 1 V than OCP for both alloys. Ti-6Al-4V alloy showed a higher corrosion resistance (higher R_p and lower I_{corr}) over Ti-15Mo alloy at both OCP and 1 V, as inferred from EIS and potentiodynamic polarization measurements. The inhomogeneity parameter and thickness values were also greater for Ti-6Al-4V alloy.

References

1. MF Lopez, JA Jimenez, A Gutierrez, *Electrochimica Acta* 48 (2003) 1395-1401.
2. I Milosev, M Metikos-Hukovic, HH Strehblow, *Biomaterials* 21 (2000) 2103-2113.

3. R Banerjee, S Nag, J Stechschulte, HL Fraser, *Biomaterials* 25 (2004) 3413-3419.
4. S Nag, R Banerjee, J Stechschulte, HL Fraser, *J Mater Sci Mater Med* 16 (2005) 679-685.
5. Y Okazaki, S Rao, Y Ito, T Tateishi, *Biomaterials* 19 (1998) 1197.
6. M Jatsy, *J Appl Biomater* 4 (1993) 273-276.
7. DM Brunette, P Tengvall, M Textor, P Thomsen, Titanium in Medicine: Material Science, Surface science, Engineering, Biological Responses and Medical Applications, Springer, (2001).
8. M Karthega, V Raman, N Rajendran, *Acta Biomaterialia* 3 (2007) 1019-1023.
9. MV Popa, I Demetrescu, E Vasilescu, PDAS Lopez, J Mirza-Rosca, C Vasilescu, D Ionita, *Electrochim Acta* 49 (2004) 2113-2121.
10. T Hanawa, *Sci. Technol. Adv. Mater*. 3(4), 289 (2002) 289–295.
11. M Long, HJ Rack, *Biomaterials* 19, (1998) 1621-1639.
12. AC Fraker, in Corrosion Tests and Standards: Application and Interpretation, ed. by R. Baboian, ASTM manual series, (1995).
13. Y Oshida, Bioscience and Bioengineering of Titanium Materials, Elsevier, 1st edition, (2007) 25.
14. J Black, in Biological Performance of Materials: Fundamentals of Biocompatibility, Marcel Decker, New York, NY, USA, (1992) 38-60.
15. M Pourbaix, Atlas of Electrochemical Equilibria in Aqueous Solutions, London: Pergamon Press Ltd, (1966).
16. M Pourbaix, Atlas of Electrochemical Equilibria in Aqueous Solutions, 2nd. edition. NACE International, Houston, TX (1974).
17. CH Hsu, F Mansfeld, *Corrosion* 57 (2001) 747-748.
18. S Chongdar, G Gunasekaran, P Kumar, *Electrochimica Acta* 50 (2005) 4655
19. GT Burstein, RM Souto, *Electrochim. Acta* 40 (1995) 1881–1888.
20. SM Bhola, R Bhola, B Mishra, DL Olson, *J Mater Sci,* 45(22) (2010) 6179-6186.
21. SM Bhola, R Bhola, B Mishra, DL Olson, *J Mater Sci: Mater in Medicine,* 22(4) (2010) 773-779.
22. SM Bhola, S Kundu, F Alabbas, B Mishra, DL Olson, *Int J of Electrochem Sci,* 8 (2013) 5172-5182.
23. R Bhola, SM Bhola, B Mishra, DL Olson, *Trends in Biomaterials & Artificial Organs,* 25(1) (2011) 34-46.
24. MA Abdel-Rahim, *J Appl Electrochem* 25(9) (1995) 881-885.
25. R Wen-Wei Hsu, CC Yang, CA Huang, YS Chen, *Mater Chemi Phy*, 86, (2004) 269-278.